

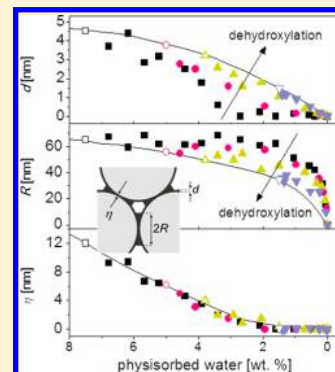
In Situ Optical Study of Water Sorption in Silica Colloidal Crystals

Francisco Gallego-Gómez,* Alvaro Blanco, and Cefe López

Instituto de Ciencia de Materiales de Madrid, C/Sor Juana Inés de la Cruz 3, 28049 Madrid, Spain

S Supporting Information

ABSTRACT: We apply a recent optical technique to investigate fundamental water adsorption/desorption phenomena on submicrometer Stöber silica sphere surfaces of varying hydrophilicity. Thermally annealed (partially dehydroxylated) silica colloidal crystals are used as test systems for the sensitivity of their photonic properties to water. The allocation of physisorbed water on the crystal spheres is inferred in situ during water desorption by simple optical spectroscopy. Silica dehydroxylation and water desorption were found to have dissimilar effects on the water distribution, which is therefore unique for each hydrophilicity and hydration state. Physisorbed water in hydrophilic (fully hydroxylated) compacts tended to accumulate between adjacent spheres forming large necks, whereas it distributed more uniformly (small necks) in hydrophobic (dehydroxylated) ones. Counterintuitively, water films on the spheres surface were released faster upon desorption in the case of hydrophilic crystals. With this exception, water desorption was identical irrespective of silica hydroxylation or water content. Remarkably, the separation between spheres in the nonclose-packed crystals exclusively depended on water content and not on hydrophilicity. These results are compatible with water transport from the spheres surface to the necks, which is gradually hindered in hydrophobic crystals. Our method revealed extreme accuracy allowing us to measure nanometer-scale changes like thin surface water films (from 5 to 0 nm) or slight sphere shrinkage upon annealing of less than 2% (4 to 7 nm), which are hardly discernible with other techniques like dynamic light scattering or electron microscopy.



INTRODUCTION

Colloidal silicas are present in many industrial and scientific fields like electronics, catalysis, glass and ceramics, chromatography, health care, etc.^{1,2} Due to the hydrophilic character of silica, molecular water from the surrounding moisture is adsorbed on the colloid surface through hydrogen bonds to silanol groups (physisorption).^{2–4} Water adsorption on silica surfaces and posterior desorption play a prime role in the physical properties of many colloidal systems^{1,2,5} and important phenomena like wetting and spreading^{6,7} on silica surfaces. However, many aspects are still unclear to-date.^{8–10} A main difficulty is the lack of techniques allowing the investigation of the water–silica interface at the nanometer scale. Thus, studies in colloid science have typically been restricted to scales ranging from several micrometers to one millimeter. Moreover, in situ characterization of water distribution within such systems is most desirable in order to investigate dynamic phenomena.

Recently, a new method¹¹ has been reported to investigate the distribution of adsorbed water in silica colloidal crystals, profiting from their particular optical properties. There, the photonic stop-band, which is a certain wavelength range in which light cannot propagate in all directions, was employed as a monitoring tool. The strong dependence of the stop-band on the water adsorbed in the crystal, not only on the amount but also on its distribution, was exploited to determine how water is placed around the silica spheres (in the crystal interstices) and between them. This method was further used to monitor in situ the water desorption upon moderate heating of the crystal, showing the evolution of the water pattern in the nanometer

range. Specifically, these results contributed to deeper knowledge on aspects of artificial opals. Here we show this technique to be a powerful tool to study fundamental water–silica phenomena in nanostructures like water adsorption/desorption on different silica surfaces.

In this study we investigate the influence of the silica surface by measuring how the water pattern changes in annealed silica colloidal crystals. Thermal annealing is known to modify the silica surface chemistry as surface silanols are progressively eliminated (dehydroxylation).^{2,3} As a result, silica becomes less hydrophilic and, thus, less capable to uptake water from moisture. It has recently been shown¹² that the amount of physisorbed water moderately decreased in silica colloidal crystals subjected to annealing temperatures (T_a) between 150 and 400 °C, whereas it drastically diminished at higher temperatures. Thus we subjected here colloidal crystals to $T_a > 400$ °C, so that silica hydrophobicity was significantly increased. Nevertheless, T_a did not surpass 600 °C in order to minimize (1) removal of water from inside the silica spheres due to condensation of internal silanols^{2,12} and (2) sintering leading to spheres deformation or specific surface change.^{2,13,14} These effects may change the silica refractive index and opal morphology,^{14,15} complicating the data analysis. The employed colloidal crystals were made of Stöber spheres. Although Stöber-synthesized silica exhibits particular characteristics

Received: April 20, 2012

Revised: August 6, 2012

Published: August 6, 2012

compared to other silica types (see the Supporting Information), the dehydroxylation process in all cases is similar,^{16,17} so the general results reported in the literature on this respect are assumed. The typical ultramicroscopic structure of Stöber spheres¹⁸ makes difficult a detailed characterization of population and types of silanol groups. An estimate of silanol densities is made from thermogravimetry. Nevertheless, quantitative data are not required along this analysis which allows our study to be carried out by purely optical means.

■ EXPERIMENTAL METHODS

Colloidal Crystal Photonic Properties. Solid colloidal crystals of self-assembled spheres (also referred to as artificial opals) are widely employed as inexpensive and versatile photonic crystals.¹⁹ In particular, opals made of submicrometer Stöber silica spheres ordered in a face centered cubic (fcc) packing²⁰ are commonly used because of the ease of fabrication. Their photonic properties depend not only on the size and packing of the spheres but also on both refractive indices of the silica spheres (n_{sphere}) and of the opal voids (interstices) surrounding the spheres (n_v). These properties were inferred from the position and width of the Bragg peak (the lowest energy stop-band, associated to the diffraction at the (111) crystallographic planes). Its position (λ_{Bragg}) is described in a good approximation by Bragg's law, given at normal incidence by

$$\lambda_{\text{Bragg}} = 2d_{111}\sqrt{fn_{\text{sphere}}^2 + (1-f)n_v^2}$$

where the lattice parameter d_{111} is the spacing of the (111) planes and f is the filling fraction of the spheres. In ideal (close-packed) fcc structures, $f = 0.74$ and $d_{111} = (2/3)^{1/2} D$. n_{sphere} is 1.43 (ref 15); n_v depends on the media filling the crystal voids, in our case, air and physisorbed water (with a filling fraction f'), and it is given by

$$n_v = \sqrt{f'n_{\text{water}}^2 + (1-f')n_{\text{air}}^2}$$

where n_{water} and n_{air} are the refractive indices of water (1.33) and air (1.0), respectively. The experimental stop-bandwidth was obtained from the full-width at half-maximum (fwhm) of the Bragg peak.

Crystals Fabrication and Annealing. Silica colloidal crystals were prepared from dilute ethanol colloidal suspensions of monosized Stöber silica spheres²¹ (with diameter D of 335 nm, 3% polydispersity) following the vertical deposition method on the glass substrate under controlled temperature and humidity conditions.¹¹ High-quality (maximum reflectance close to 80%) crystals were obtained, with an average size of >2 cm² and formed by ~ 30 monolayers. Pieces of as-grown samples were annealed in air at different temperatures ($T_a = 435, 510, \text{ and } 560$ °C) in a conventional oven by slowly heating (1 °C/min) up to T_a , waiting for 3 h, and cooling (10 °C/min) to room temperature (RT = 22 °C). Before measurements, annealed samples were stored under ambient conditions (RT, $\sim 35\%$ humidity) for at least one day to allow complete moisture adsorption (full hydration). Silica surface rehydroxylation is known to occur after thermal annealing, even in ambient conditions, mainly if T_a did not surpass ~ 500 °C.^{2,3} Indeed, partial rehydroxylation of our samples was noticed, which evolved relatively slowly within the first 6–8 d and speeded up in the successive weeks (see the Supporting Information, S1). Therefore, measurements were performed

within the first week after annealing in order to have a fairly constant hydroxylation state. Nevertheless, similar qualitative results were obtained after sample storage times longer than 4 weeks. Compacts quality was checked before and after annealing by scanning electron microscopy, SEM (FEI Nova NANOSEM 230).

Heating Experiment and in Situ Reflection Spectroscopy. The colloidal crystal stop-band was characterized by measuring reflectance with an Ocean 2000+ spectrometer using white light (halogen lamp Osram HLX 64623). The crystal was set on a hot plate for controlled sample heating while reflection spectra were simultaneously measured.¹¹ To measure the effect of water desorption, each sample was heated by increasing the hot plate temperature stepwise from RT to 200 °C. Each temperature was maintained for 30 min before measurement in order to ensure thermal equilibrium in the sample. Prior to any measurement, each crystal was slightly heated (up to 60 °C) and cooled to RT. During this "initializing" cycle, stop-band changes (principally in as-grown samples) were rather irreversible and showed poor reproducibility in different samples. This was presumably related to evaporation of excess of water in liquid phase (free water), which was in suspension and cannot be associated with desorption of water.³ Changes in further cycles were then reversible and reproducible.

Experimental data were compared with theoretical calculations (MPB software²²) of the stop-band in fcc crystals with different water distribution in order to obtain the best agreement.¹¹ As finite size effects can be disregarded in silica colloidal crystals above 10–15 layers,²³ infinite-media MPB computations could be directly compared with measurements in our 30-layers samples. The analysis assumed isotropic fcc crystals formed by perfect spheres and isotropic deformations upon water removal. Moreover, disorder effects were excluded, which was justified by the high stop-band reflectance even after annealing and during heating experiments (close to 80%).

■ RESULTS AND DISCUSSION

Thermally Annealed Crystals. Thermal annealing provided, upon silica surface dehydroxylation, crystals formed by increasingly hydrophobic silica spheres (before measurements, samples were allowed to fully hydrate; see Experimental Methods). Structural characterization has been performed on as-grown and annealed Stöber spheres by infrared spectroscopy, thermogravimetry (TGA) and nitrogen porosimetry (Supporting Information, Figures S2–S4 and Table S1). Annealing preserved crystalline order and the spheres morphology remained unaltered at microscopic scale (Figure 1a,b). Indeed, room-temperature optical spectroscopy (see Figure S5) shows that the stop-band reflectance ($\sim 80\%$) barely decreased, which indicates that the annealing did not induce substantial structural defects. However, the notable stop-band changes demonstrated that the crystals were permanently modified in a significant way. Annealing greatly affected water physisorption but barely changed the content of water inside the spheres, as demonstrated by TGA.¹² The amount of physisorbed water contained in each crystal and its temperature-dependent removal by desorption (Figure 1c) is calculated from the weight loss during crystal heating from RT to 200 °C.¹² As expected, water uptake markedly decreased in annealed films as silica became gradually hydrophobic with increasing T_a . At RT (full hydration) the physisorbed water content reduced from 7.5 to 1.5 wt % after 560 °C-annealing

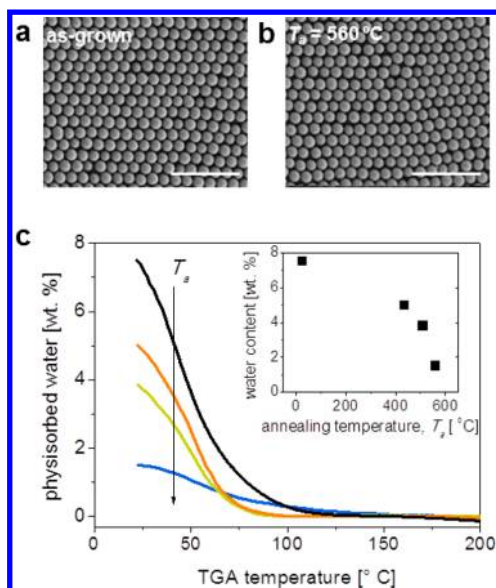


Figure 1. SEM micrographs of as-grown (a) and 560 °C annealed crystals (b) (scale bar is 2 μm). (c) Temperature-dependent physisorbed water content in as-grown and annealed crystals as obtained from thermogravimetric measurements. Inset: physisorbed water content at RT as function of T_a . The arrow in panel c indicates increasing T_a : RT (no annealing, back line) and annealed at 435, 510, and 560 °C (colored lines).

(inset in Figure 1c). Water was completely desorbed in all crystals by heating at 120–150 °C.

Water-Dependent Stop-Band Changes and In-Situ Optical Measurement of Water Desorption. As reported in ref 11, it is possible to infer the spatial distribution of water adsorbed in a colloidal crystal from both stop-band position (λ_{Bragg}) and width (fwhm) if the water content is known (e.g., from TGA or IR absorbance¹²). Measuring the stop-bands at RT informs about the differences between water patterns in fully hydrated as-grown and annealed compacts (Figure S6). By monitoring in situ the stop-band during sample heating (Figure 2), we obtain the crystal evolution upon removal of the physisorbed water until complete dehydration. This informs us about water desorption in silica crystals with different hydrophilicity. Besides, this procedure has a crucial advantage as the data examination does not only depend on the fitting of one-point measurement but of a whole data set for each crystal, minimizing analysis errors. It is worth remarking that, during crystal heating, the spheres surface chemistry remained unchanged as no dehydroxylation occurs in this temperature range.

Figure 2 shows strong differences in the stop-band behavior of the annealed crystal. On the one hand, at RT (first points of each data set), the stop-band after thermal annealing significantly shifted to shorter wavelengths (over 40 nm) and narrowed (up to 13%). The decrease of fwhm denotes that the gradual reduction of water adsorption led to compaction of the nonclose-packed spheres arrangement.^{11,12} On the other hand, the stop-band evolution upon heating became smoother in increasingly dehydroxylated compacts (increasing T_a), although the general trend was the same: simultaneous decrease of λ_{Bragg} and fwhm. The evolution with heating resembled the water desorption curves in Figure 1c, which evidence the close correlation between both phenomena. Again, fwhm decrease indicates contraction of the nonclose-packed structure, due to

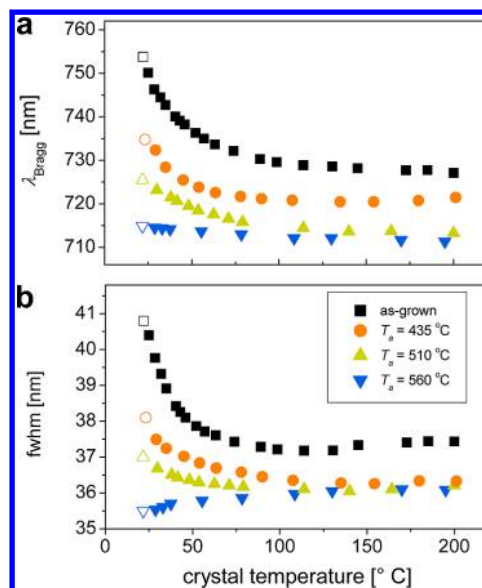


Figure 2. Evolution upon crystal heating of (a) λ_{Bragg} and (b) fwhm of the photonic bandgap in as-grown (black symbols) and annealed crystals (colored symbols). Open symbols correspond to the values measured at RT.

the heat-induced water desorption.¹¹ As a remarkable exception, fwhm in the 560°-annealed sample increased upon heating, suggesting in this case a close-packed arrangement at RT. Changes due to desorption were essentially reversible, so the Bragg peak tended toward its original form and position upon cooling.

In Figure 3, the stop-band evolution is plotted against the physisorbed water content until complete desorption (x axis

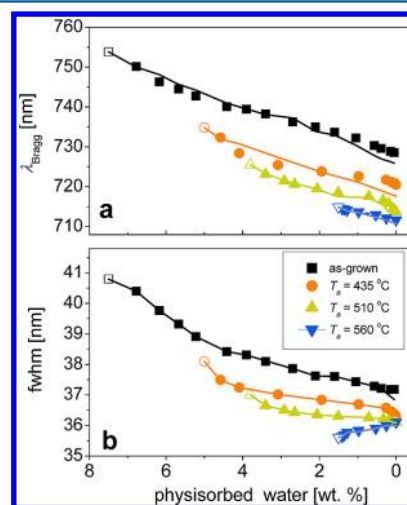


Figure 3. Experimental data, combining Figures 1c and 2, of (a) λ_{Bragg} and (b) fwhm for progressive loss of physisorbed water in as-grown (black symbols) and annealed crystals (colored symbols). Lines are fitting curves of the model.

shows decreasing water content, which is the change direction in the heating experiment). This representation demonstrates, on the one hand, that the stop-bands did not coincide at same water contents; that is, the crystal photonic properties depended on the silica hydroxylation state. On the other hand, data evolved nearly parallel to each other, indicating that the smoother stop-band change in annealed crystals reflected

the reduced extent of water removal. In general, stop-band data monotonously decreased, more prominently at the initial water loss and also at vanishing water contents. The 560 °C-annealed crystal, in which fwhm increased, was the exception.

Fitting of Experimental Data. We distinguish between (i) water located in the crystal interstices, building up a film of thickness d over the spheres surface, and (ii) water between nearest neighbor spheres forming necks (liquid bridges).¹¹ Water necks are simply modeled by a biconcave disk of radius R (delimited by the two adjacent spheres) and width η (at its center), which also determines the distance between the spheres (Figure 4, inset).²⁴ The model parameters $\{d, R, \eta\}$,

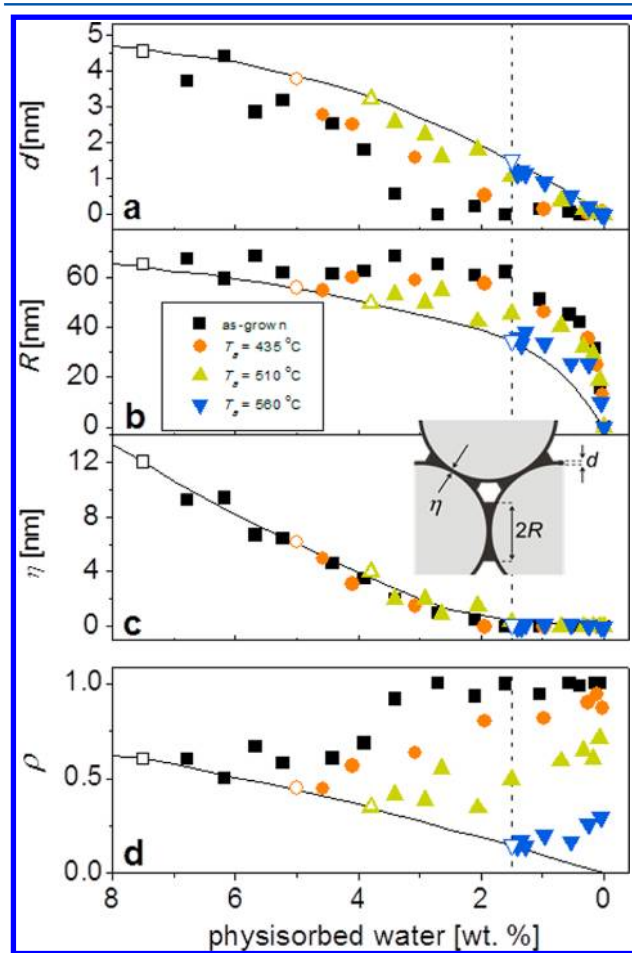


Figure 4. Evolution of the model parameters upon water removal as obtained from fitting of experimental data in as-grown (black symbols) and annealed crystals (colored symbols). Open symbols correspond to the values at RT, graphically represented in Figure 5, left (solid lines are guide-to-the-eye). Dashed lines denote crystal states at same water content (1.5 wt %), graphically in Figure 5, right. Inset in panel c outlines the modeled water distribution depicting the parameters d (thickness of water film surrounding the spheres) and R and η (describing the water necks between spheres).

which completely describe the spatial distribution of physisorbed water in the crystal, were found by iterative MPB calculations to obtain the best fit to the experimental data.¹¹ We consider a further parameter, the ratio of water in the necks to the total water (ρ), which is a function of $\{d, R, \eta\}$. This ratio is useful to illustrate whether the water is uniformly distributed in the interstices (i.e., entirely placed in the film over the spheres

without forming necks, $\rho \rightarrow 0$) or it accumulates between the spheres (building exclusively necks, $\rho \rightarrow 1$).

Regarding the procedure followed in ref 11, we make here two modifications. First, we assume complete desorption of physisorbed water at about 200 °C (Figure 1c). Above this temperature, although superficial water is further removed from the crystal, this should be identified as structurally bound surface water (released upon silanol condensation) rather than as physisorbed water.¹² This form of water has been often considered as strongly bonded adsorbed water or as chemically adsorbed (chemisorbed) water, requiring heating above 200 °C to be removed.^{4,25,26} In any case, since this water form surely has different physicochemical properties than physisorbed water, we find it more appropriate not to consider it in this analysis. Second, no satisfactory fitting was found by assuming the same spheres diameter (D) for all crystals. Therefore, we use D as a further adjustable parameter for each crystal (i.e., for each T_a) but being kept constant along the heating experiment. This is justified since the beads size might be susceptible to change upon thermal annealing (see discussion below) but not upon heating up to 200 °C.

Figure 3 demonstrates a very good agreement between fitting curves and measurements in as-grown and annealed compacts along the whole range. It must be mentioned that the results here obtained for as-grown crystals compare well with those reported in ref 11, despite the procedure modifications discussed above.

Effect of the Silica Surface on Water Adsorption/Desorption. The resulting parameters $\{d, R, \eta\}$, which describe the water distribution, and the ratio ρ are shown in Figure 4. The influence of the silica state (i.e., hydrophilicity/hydrophobicity of the surface) on these parameters is difficult to analyze because dehydroxylation in annealed crystals is accompanied by changes merely due to the reduction of adsorbed water (e.g., the overall reduction of $\{d, R, \eta\}$). In this regard, heating experiments are very helpful to compare the evolution of a single crystal (constant surface state) upon decreasing water content. At first glance, it is evident in Figure 4 that the parameters of each crystal (with the exception of η) evolved upon water desorption without overlapping with the values of any other crystal at any water content. This indicates that the increasingly surface dehydroxylation has a dissimilar effect than water desorption. In other words, two different crystals cannot present the same water pattern at any conditions: the water distribution in a silica colloidal crystal is unique and determined by the silica surface state.

We analyze in separate subheadings how water distributes in the crystals, first, at the same degree of hydration (in particular, at full hydration, i.e., at RT, Figure 5, left) and, second, along desorption upon heating (decreasing degree of hydration). Finally, we find it appropriate to compare crystals at the same water content, i.e., crystals with increasing hydrophobicity compensated by decreasing degrees of hydration (Figure 5, right) to better discern the influence of the silica surface state on the water distribution. The ratio ρ will be particularly useful since it is a normalized parameter independent of the water content.

(i). *Fully Hydrated Crystals: Physisorbed Water at RT.* Values of $\{d, R, \eta\}$ obtained at RT (first points of each data set in Figure 4) decreased in well-defined trends with T_a , tending toward 0 at increasing dehydroxylation (vanishing capability to adsorb water). The corresponding water patterns are graphically shown in Figure 5, left. Spheres progressively approached

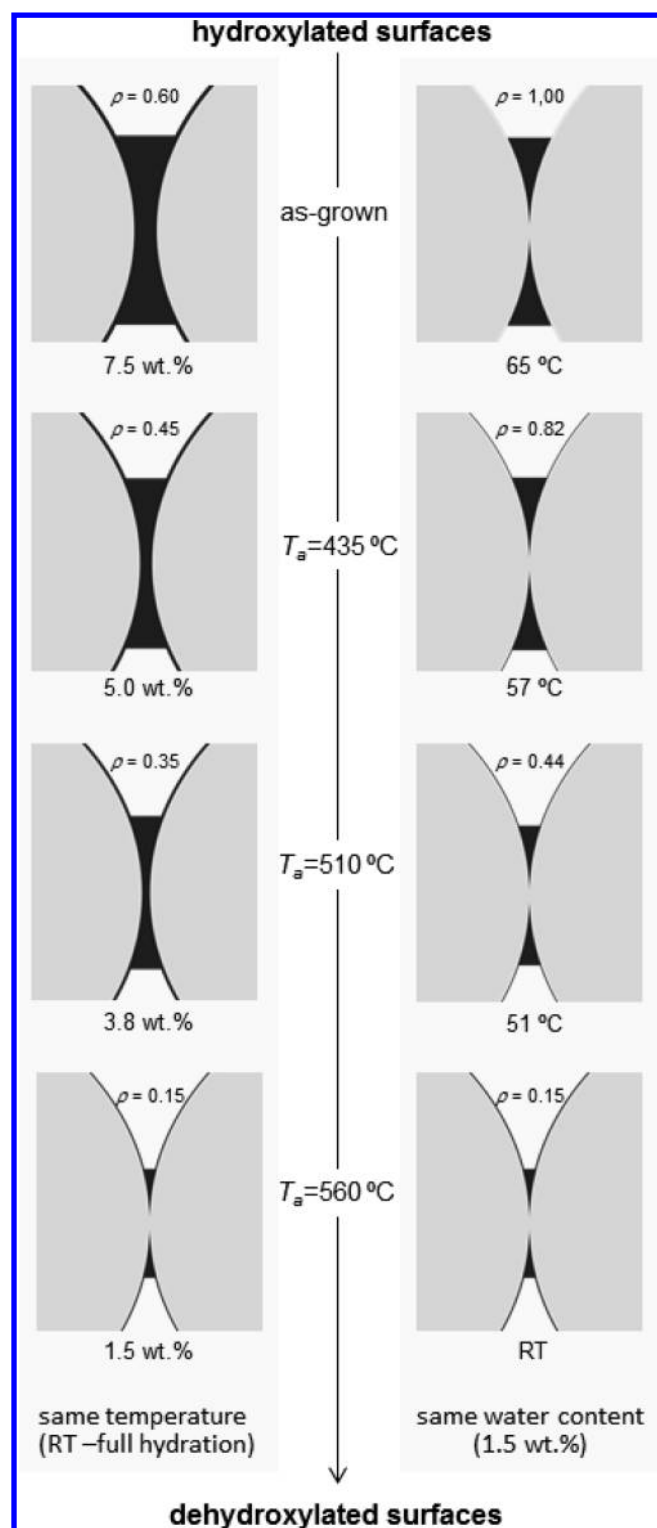


Figure 5. Off-cut side view of two nearest neighbor spheres according to the parameters obtained in Figure 4 (all proportions are maintained). The change of water pattern is shown, from top to bottom, in progressively dehydroxylated crystals. Left column: crystals at the same degree of hydration, i.e., same sample temperature (in particular, full hydration at RT, solid lines in Figure 4). Right column: crystals at different temperatures to have the same water content (1.5 wt %, dashed lines in Figure 4). In each sketch, corresponding water content/temperature and ρ are given. From the model adopted for MPB calculations, water necks are drawn with flat edges (instead of menisci).

to each other (η reduced from 12 to ~ 0), so the crystal finally adopted a close-packed structure after annealing at 560 °C.²⁷ The thickness d of the water film decreased from 5 to 1.5 nm in the as-grown and the 560 °C annealed crystals, respectively. The as-grown value is in accord with thickness estimations for water surface layers on hydrophilic silica at about 35% relative humidity (2–10 nm).^{28–32} References 29 and 30 also reported a clear decrease of the film thickness on progressively dehydroxylated silica. As observed in Figure 5, left, reducing water adsorption affected more pronouncedly to the neck between the spheres (its volume decreased in a factor of 20 after treatment at $T_a = 560\text{ °C}$)³³ than to the film around them (with about a 3-fold volume loss). This is conveniently illustrated by the behavior of ρ , which reduced after dehydroxylation from 0.60 to 0.15. That is, water tended to a more uniform distribution in the annealed compacts than in the as-grown one. The same conclusions can be drawn by comparing the compacts at any constant degree of hydration.

(ii). *Gradually Dehydrated Crystals: Water Desorption Behavior.* Figure 4 shows that parameters in the different crystals evolve upon water desorption nearly parallel to each other. By plotting them, normalized to the respective maxima, as function of the degree of hydration (Figure 6), it is evident that desorption was essentially identical in all crystals, i.e., independently of the silica surface treatment, or even the initial (at RT) water content and distribution. As general features of desorption, film thickness d and neck width η steadily decreased toward 0, whereas the neck radius R only reduced in the last stage. The ratio ρ steadily increased along the heating experiment (compare, e.g., crystals between left and right columns in Figure 5, at RT and heated, respectively). This indicates that water on the spheres surface (more exposed without an adjacent sphere) desorbed more easily than that between the spheres surface.¹¹ This is in accordance with the general behavior of dehydration in porous systems, in which higher temperatures are required to remove water from crevices, where the equilibrium vapor pressure is lower.^{5,34,35}

A detailed scrutiny of Figure 6a reveals that d actually exhibited some dependence on the silica surface state and decreased less pronouncedly (as function of the degree of dehydration) in increasingly dehydroxylated crystals. That is, a larger percentage of the total water content was necessary to be evacuated in the partially dehydroxylated crystals in order to completely release the water film physisorbed on the spheres surface. Thus, d in the as-grown crystal vanished after only 60% dehydration of the total water amount (i.e., 3 wt % water still remained in the colloidal crystal in the form of water necks between spheres), whereas complete dehydration was needed in the 560 °C-annealed compact. This may suggest that molecular water is more strongly physisorbed on partially dehydroxylated than on fully hydroxylated silica surfaces, so it better resists desorption. However, this justification cannot be supported in terms of water affinity of the different types and population of surface silanols given that, as generally accepted, hydrogen-bonded vicinal silanols rather than nonbonded single and geminal silanols are the primary hydration sites.^{4,16} As annealing above 400 °C is known to completely eliminate vicinal silanols,^{2,3} one must expect a weaker interaction of water with annealed surfaces, in which only geminal and single silanols persisted, which is contradictory with Figure 6a. An alternative explanation is given in the next section.

(iii). *Crystals at Same Water Content.* In order to compare at same amounts of water, the less ability of annealed crystals to

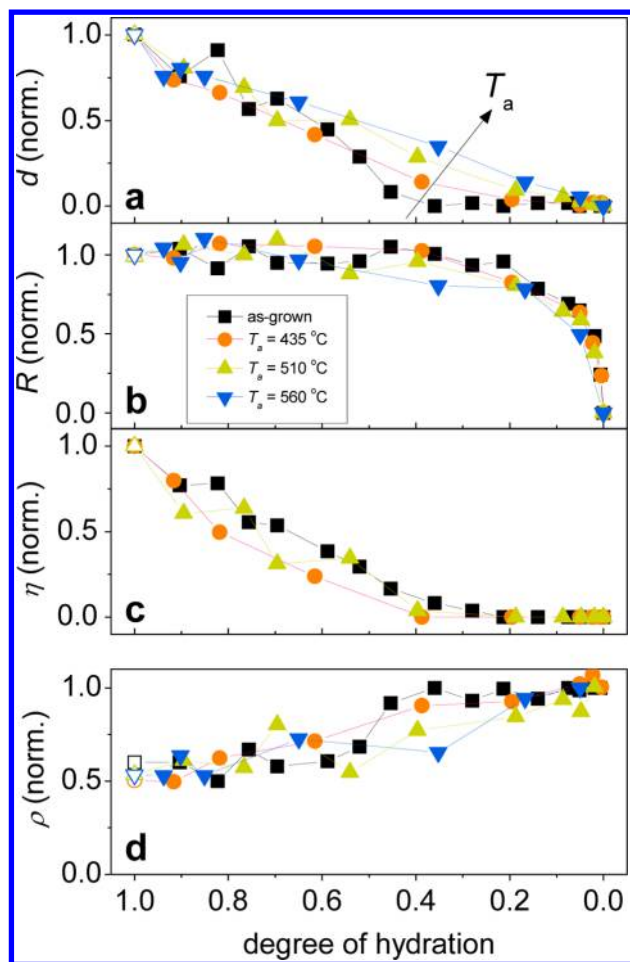


Figure 6. Normalized model parameters (from Figure 4) in as-grown (black symbols) and annealed crystals (colored symbols) as function of the degree of hydration. The degree of hydration was obtained by normalizing the water content to its maximum (at RT) in each crystal. In panel c, η of the 560 °C-annealed crystal was not included because of its vanishing values. ρ values in panel d were normalized at the smallest water content measured, since ρ is not defined in absence of water.

adsorb water is compensated by selecting higher degree of hydration (lower heating). Figures 4 (dashed line) and 5 (right column) show crystals with 1.5 wt % water (the behavior was identical for any water content). For increasing spheres dehydroxylation, we find that d increased, R decreased, and η remained constant. As a result, ρ decreased: in a hydrophilic (as-grown) crystal, water accumulated between spheres forming big necks (ρ tended to 1), whereas in hydrophobic (annealed) opals, water was distributed uniformly around the spheres, building only small necks (vanishing ρ). Note that, although the hydrophilic crystals are subjected here to higher desorption (which predominantly reduced d), this conclusion coincides with that drawn above by comparing crystals at full hydration. Indeed, both columns in Figure 5 show the decrease of ρ by increasing dehydroxylation. Such trend also agrees with the more strongly bonded water adsorbed on annealed silica surfaces, as suggested above, favoring homogeneous distribution of water and hindering accumulation in necks.

Finally, the behavior of η is remarkable, being the only parameter taking identical values in all crystals at same water contents, which is a consequence of the curves overlap in

Figure 4c. This indicates that the separation between spheres exclusively depended on the amount of physisorbed water, irrespective of the spheres surface state. Thus, the transition from nonclose- to close-packed crystal arrangement upon water desorption was equal in both as-grown and annealed crystals.

Water Transport at the Sphere Surface. Concerning the results obtained in the previous section, several considerations should be made. On the one hand, we have implicitly assumed along this work that the water film over the spheres is formed, in general, by a multilayer of water molecules with homogeneous thickness ($d > 0.3$ nm). Actually, before the multilayer is constituted, clusters of hydrogen-bonded water molecules first form around the silanols.^{17,36} This readily occurs in the as-grown crystal, in which water is abundantly adsorbed on the highly hydroxylated silica surface. However, at increasing silica dehydroxylation, the multilayer formation is not completed due to the sparseness of silanols, so the film is rather composed by isolated water clusters.^{4,29,30,37} In this context, the values obtained for d correspond to the average thickness of this inhomogeneous film. Nevertheless, the collective nature of the photonic properties of the colloidal crystal, which we used to probe the characteristics of the system, justifies the use of average thicknesses to correctly simulate the actual structure.

On the other hand, it must be kept in mind that we deal in this study with steady-state water patterns, so some water redistribution might have occurred during the experiment. In particular, the accumulation of water between spheres, among capillary condensation,^{5,34} may be due to liquid flow from the water film on the surface to the necks.^{10,38–40} Indeed, this agrees with two observations: (1) the width η of the necks depended on the amount of water rather than on the silica surface state and (2) upon heating, the neck radius R began to decrease only when the water film was completely desorbed ($d = 0$), as shown in Figure 4, and this trend held for the as-grown and the 435 °C-annealed crystals, while it started to fail at further annealing. These findings suggest water transport from the sphere surface to the necks until being hindered by the isolated water clusters on dehydroxylated silica. This is also consistent with the surface-dependent behavior of d observed in Figure 6a: during desorption, water flows from the water film into the necks in the fully hydroxylated crystal, so d vanishes more easily, whereas such transport is hindered on the gradually dehydroxylated surfaces and d persists longer. These arguments, in turn, fully agree with the finding of less accumulation of water in the necks of annealed compacts, as mentioned above.

Spheres Size Reduction upon Annealing. To conclude, it is worth mentioning that our model allowed the indirect measurement of the spheres diameter D . As mentioned above, D was adjusted for each crystal to achieve the best fit of each data set. That is, a different value of D was obtained for each T_a (Figure 7a). $D = 338$ nm was obtained for the as-grown crystal, which was very close to the nominal spheres size. The diameter decreased after annealing above 400 °C (although slightly, less than 7 nm at 560 °C), exhibiting a clear trend with T_a . The large decrease of λ_{Bragg} after annealing (Figure 2a) already pointed to such spheres size reduction. Indeed, only the compaction of the as-grown crystal structure, even completely (η decreasing from 12 to 0 nm), cannot explain blueshifts larger than 23 nm (against, e.g., 40 nm measured after annealing at 560 °C). Besides, without changing D , the stop-band properties

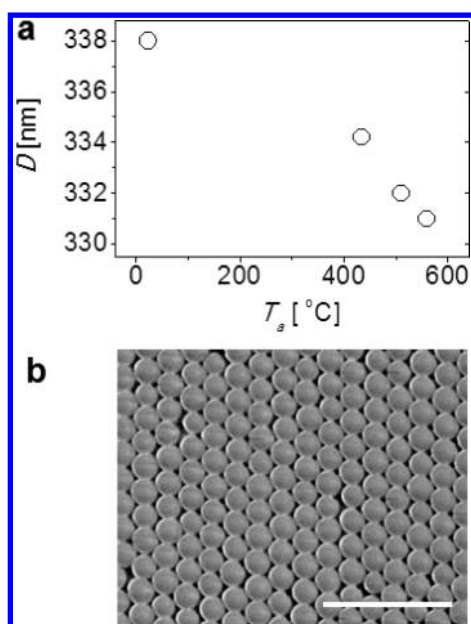


Figure 7. (a) Spheres diameter D , obtained from fitting of the experimental data, as function of the annealing temperature T_a . (b) SEM micrograph of local sintering in a 560 °C annealed crystal (scale bar is 2 μm).

of all crystals heated at 150–200 °C (i.e., at complete water desorption) must have coincided, which was not the case.

Spheres size reduction requires removal of internal water accompanied by incipient sintering leading to bulk contraction. Although both processes (particularly sintering) were expected to occur at higher temperatures (>600–700 °C), our results suggest that they can start at about 400 °C or less.⁴¹ This conclusion is further supported by the observation of evident sintering in localized spots of the 560 °C-annealed crystal (Figure 7b). This indicates that the range of T_a employed is close to induce extensive viscous flow, so sintering across ultramicropores has plausibly taken place in some degree. Note that we considered the same silica refractive index for all crystals in MPB calculations. This is justified by measurements on very similar Stöber silica spheres (reported in ref 15), which yielded constant index (with accuracy of $\sim 0.7\%$) after annealing at up to 600 °C. Such constancy is compatible with the spheres shrinkage as long as the nanopores formed upon the internal water removal (at least, part of them) remain empty. Thus, the decrease of average refractive index in the empty pores (air substituting water) can counterbalance the increase in the densified locations (silica substituting water).

The slight size reduction we measured (less than 2%) is small for the accuracy of techniques generally employed² (dynamic light scattering, surface area measurement or transmission/scanning electron microscopy (TEM/SEM)). In particular, studies using SEM measurements are contradictory, some of them reporting large silica spheres shrinkage (6–10% in diameter) after annealing at 500 °C,^{42–44} whereas others detected no changes below 600¹⁴ or 750 °C.¹⁵ This might indicate that electron microscopy is not appropriate to measure such features, due to shortcomings such as typical image artifacts, inefficient dehydration,⁴⁵ or insufficient statistics. In this regard, among the simplicity of the setup, our optical method takes advantage of simultaneously measuring many thousands of spheres, as the stop-band results from the collective order. The excellent overall agreement of the fitting

curves with the experimental data (Figure 3) supports the reliability of the obtained D values.

CONCLUSIONS

Here we have investigated in situ fundamental features of water adsorption/desorption on Stöber silica surfaces with a novel approach. Hereby, we have applied a recent optical technique to annealed silica colloidal crystals in order to infer the water distribution over the spheres depending on the silica surface dehydroxylation. By analyzing the stop-band changes after annealing and during heat-induced water desorption, we demonstrated that the water distribution in a silica colloidal crystal was unique and determined by the silica surface state.

The influence of the silica hydroxylation state on the water distribution over the spheres can be summarized in two main conclusions: (i) In a hydrophilic (as-grown) compact, water accumulated between spheres forming large liquid necks, whereas in hydrophobic (dehydroxylated) silica crystals, water distributed uniformly building only slight necks. (ii) Upon desorption, the water film on the spheres persisted longer (higher degree of dehydration was needed) on dehydroxylated than on as-grown silica. By contrast, the evolution of water desorption was essentially unaffected by the silica surface: in all cases, water evaporation was more pronounced in the crystal interstices than between spheres. Moreover, the separation between crystal spheres was also independent of the surface state, so the nonclose-packed crystal arrangement was only governed by the water content. These results were compatible with liquid transport from the surface water films to the necks between spheres, which appears to be favored in fully hydroxylated crystals and progressively hindered in annealed ones.

In conclusion, accurate investigation of liquid/solid interface phenomena in submicrometer colloidal structures using simple in situ optical characterization has been proved, being sensitive to nanometer-scale changes. This is well illustrated by measuring thin water films (from 5 to 0 nm) or slight spheres shrinkage upon annealing of less than 2% (4–7 nm), hardly discernible with standard techniques. Despite the structural differences of Stöber silica compared to other silica types, the outer surface of the spheres should exhibit universal silica characteristics like the Kiselev-Zhuravlev surface silanol density (~ 4.9 units/nm² in fully hydroxylated surfaces).^{2,3} Thus, our results are expected to be valid in systems made of other silica types, although this must be confirmed by further experiments. Also, some results compared well with measurements of water adsorption in other silica systems like flat plates or wedges, a fact which supports our approach to be a useful tool for general interface investigations. New insights on adsorption–desorption phenomena have been provided, being of relevance not only for colloid science but also for many fields involving capillary condensation, like scanning microscopy,⁴⁶ wetting research,⁴⁷ and generic granular materials.^{35,48}

ASSOCIATED CONTENT

Supporting Information

Structural characterization and estimate of silanol densities of the Stöber silica spheres, rehydroxylation dynamics, and UV–vis spectra of the colloidal crystals. This material is available free of charge via the Internet at <http://pubs.acs.org>.

■ AUTHOR INFORMATION

Corresponding Author

*E-mail: francisco.gallego@icmm.csic.es.

Notes

The authors declare no competing financial interest.

■ ACKNOWLEDGMENTS

F.G.-G. was supported by the JAE Postdoctoral Program from the CSIC. This work was partially supported by EU FP7 NoE Nanophotonics4Energy Grant No. 248855; the Spanish MICINN CSD2007-0046 (Nanolight.es), MAT2009-07841 (GLUSFA), and Comunidad de Madrid S2009/MAT-1756 (PHAMA) projects.

■ REFERENCES

- (1) Pashley, R. M.; Karaman, M. E., Eds.; *Applied Colloid and Surface Chemistry*; John Wiley & Sons, Ltd.: West Sussex, 2004.
- (2) Bergna, H. E.; Roberts, W. O. *Colloidal Silica: Fundamentals and Applications*; CRC Press Taylor and Francis: Boca Raton, 2006.
- (3) Zhuravlev, L. T. *Colloid Surf. A* **1993**, *74*, 71–90.
- (4) Papirer, E., Ed.; *Adsorption on Silica Surfaces*; Marcel Dekker Inc.: New York, 2000.
- (5) Butt, H. J.; Kappl, M. *Surface and Interfacial Forces*; Wiley-VCH Verlag: Weinheim, 2010.
- (6) de Gennes, P. G. *Rev. Mod. Phys.* **1985**, *57*, 827–863.
- (7) Kumar, G.; Prabhu, K. N. *Adv. Colloid Interface Sci.* **2007**, *133*, 61–89.
- (8) Panella, V.; Chiarello, R.; Krim, J. *Phys. Rev. Lett.* **1996**, *76*, 3606–3609.
- (9) Müller, H. J. *Langmuir* **1998**, *14*, 6789–6792.
- (10) Maeda, N.; Israelachvili, J. N.; Kohonen, M. M. *Proc. Natl. Acad. Sci. U.S.A.* **2003**, *100*, 803–808.
- (11) Gallego-Gómez, F.; Blanco, A.; Canalejas-Tejero, V.; López, C. *Small* **2011**, *7*, 1838–1845.
- (12) Gallego-Gómez, F.; Blanco, A.; Golmayo, D.; López, C. *Langmuir* **2011**, *27*, 13992–13995.
- (13) Vasconcelos, W. L.; DeHoff, R. T.; Hench, L. L. *J. Non-Cryst. Solids* **1990**, *121*, 124–127.
- (14) Miguez, H.; Meseguer, F.; López, C.; Blanco, A.; Moya, J. S.; Requena, J.; Mifsud, A.; Fornés, V. *Adv. Mater.* **1998**, *10*, 480–483.
- (15) Garcia-Santamaria, F.; Miguez, H.; Ibisate, M.; Meseguer, F.; Lopez, C. *Langmuir* **2002**, *18*, 1942–1944.
- (16) Legrand, A. P. *The Surface Properties of Silicas*; J. Wiley & Sons: New York, 1998.
- (17) Burneau, A.; Barres, O.; Gallas, J. P.; Lavalley, J. C. *Langmuir* **1990**, *6*, 1364–1372.
- (18) van Helden, A. K.; Jansen, J. W.; Vrij, A. *J. Colloid Interface Sci.* **1981**, *81*, 354–368.
- (19) Galisteo-López, J. F.; Ibisate, M.; Sapienza, R.; Froufe-Pérez, L. S.; Blanco, A.; López, C. *Adv. Mater.* **2011**, *23*, 30–69.
- (20) Miguez, H.; Meseguer, F.; López, C.; Mifsud, A.; Moya, J. S.; Vazquez, L. *Langmuir* **1997**, *13*, 6009–6011.
- (21) Stöber, W.; Fink, A.; Bohn, E. *J. Colloid Interface Sci.* **1968**, *26*, 62–69.
- (22) MIT Photonic Bands (MPB) software. Johnson, S. G.; Joannopoulos, J. D. *Opt. Express* **2001**, *8*, 173–190.
- (23) Bertone, J. F.; Jiang, P.; Hwang, K. S.; Mittleman, D. M.; Colvin, V. L. *Phys. Rev. Lett.* **1999**, *83*, 300–303.
- (24) According to this, water necks are assumed to be delimited by flat edges instead of concave menisci because the latter cannot be implemented in MPB calculations.
- (25) Sindorf, D. W.; Maciel, G. E. *J. Phys. Chem.* **1983**, *87*, 5516–5521.
- (26) Sacks, M. D.; Tseng, T.-Y. *J. Am. Ceram. Soc.* **1984**, *67*, 526–532.
- (27) Note that the 560 °C annealed crystal is the only case of stop-band broadening upon posterior water desorption (Figures 2 and 3).
- (28) Garbatski, U.; Folman, M. *J. Phys. Chem.* **1956**, *60*, 793–796.
- (29) Pashley, R. M.; Kitchener, J. A. *J. Colloid Interface Sci.* **1979**, *71*, 491–500.
- (30) Gee, M. L.; Healy, T. W.; White, L. R. *J. Colloid Interface Sci.* **1990**, *140*, 450–465.
- (31) Grabbe, A.; Horn, R. G. *J. Colloid Interface Sci.* **1993**, *157*, 375–383.
- (32) Mazzoco, R. R.; Wayner, P. C., Jr. *J. Colloid Interface Sci.* **1999**, *214*, 156–169.
- (33) Note that the shape of the water necks also changed, becoming clearly narrower. This can be quantified by the aspect ratio η/R , decreasing from 0.19 to 0.
- (34) Israelachvili, J. N. *Intermolecular and Surface Forces*, 2nd ed.; Academic Press: London, 1992.
- (35) Bocquet, L.; Charlaix, E.; Ciliberto, S.; Crassous, J. *Nature* **1998**, *396*, 735–737.
- (36) Klier, K.; Zettlemoyer, A. C. *J. Colloid Interface Sci.* **1977**, *58*, 216–229.
- (37) Klier, K.; Shen, J. H.; Zettlemoyer, A. C. *J. Phys. Chem.* **1973**, *77*, 1458–1465.
- (38) Maeda, N.; Kohonen, M. M. *J. Phys. Chem. B* **2001**, *105*, 5906–5913.
- (39) Seemann, R.; Mönch, W.; Herminghaus, S. *Europhys. Lett.* **2001**, *51*, 698–704.
- (40) Tokunaga, T. K. *Water Resour. Res.* **2011**, *47*, W08514.
- (41) Some authors, in fact, claim that sintering starts at 400 °C. See, e.g., Hench, L. L.; Wang, S. H. *Phase Transit.* **1990**, *24–26*, 785–834.
- (42) Chabanov, A. A.; Jun, Y.; Norris, D. J. *Appl. Phys. Lett.* **2004**, *84*, 3573–3575.
- (43) Van Le, T.; Ross, E. E.; Velarde, T. R. C.; Legg, M. A.; Wirth, M. *J. Langmuir* **2007**, *23*, 8554–8559.
- (44) Liu, K.; Schmedake, T. A.; Tsu, R. *Phys. Rev. Lett. A* **2008**, *372*, 4517–4520.
- (45) In water-containing systems, desorption in vacuum might not be exhaustive before measurement. In colloidal silica crystals (as-grown, principally), incomplete dehydration would lead to overestimation of D , as some adsorbed water may remain between spheres.
- (46) Köber, M.; Sahagún, E.; García-Mochales, P.; Briones, F.; Luna, M.; Sáenz, J. *J. Small* **2010**, *6*, 2725–2730.
- (47) Méndez-Vilas, A.; Jódar-Reyes, A. B.; González-Martín, M. L. *Small* **2009**, *5*, 1366–1390.
- (48) Herminghaus, S. *Adv. Phys.* **2005**, *54*, 221–261.